Orbital-ordering driven structural distortion in metallic $SrCrO_3$.

K.-W. Lee[1,2] and W. E. Pickett[1]
[1] *Department of Physics, University of California, Davis, CA 95616, USA*
[2] *Department of Display and Semiconductor Physics, Korea University, Jochiwon, Chungnam 339-700, Korea*
(Dated: May 5, 2009)

In contrast to the previous reports that the divalent perovskite $SrCrO_3$ was believed to be cubic structure and nonmagnetic metal, recent measurements suggest coexistence of majority tetragonally distorted weak antiferromagnetic phase and minority nonmagnetic cubic phase. Within the local spin density approximation (LSDA) our calculations confirm that a slightly tetragonally distorted phase indeed is energetically favored. Using the correlated band theory method (LDA+ Hubbard U) as seems to be justified by the unusual behavior observed in $SrCrO_3$, above the critical value U_c=4 eV only the distorted phase undergoes an orbital-ordering transition, resulting in $t_{2g}^2 \rightarrow d_{xy}^1(d_{xz}d_{yz})^1$ corresponding to the filling of the d_{xy} orbital but leaving the other two degenerate. The Fermi surfaces of the cubic phase are simple with nesting features, although the nesting wavevectors do not correlate with known data. Fixed spin moment calculations indicate the cubic structure is just beyond a ferromagnetic Stoner instability ($IN(0) \approx$1.1) in LSDA, and that the energy is unusually weakly dependent on the moment out to 1.5μ_B/Cr (varying only by 11 meV/Cr), reflecting low energy long-wavelength magnetic fluctuations. We observe that this system shows strong magneto-phonon coupling (change in Cr local moment is $\sim$7.3 μ_B/Å) for breathing phonon modes.

PACS numbers: 71.20.Be, 71.30.+h, 75.50.Ee

I. INTRODUCTION

Forty years ago, a few divalent chromate perovskites $\mathcal{A}CrO_3$ ($\mathcal{A}$=Pb, Sr, Ca), formally possessing the Cr^{4+} ion, were synthesized at high temperature $\sim$1300 K and under high pressure 6–10 GPa by a few groups.[1–5] In spite of their atypical and controversial properties, these systems have been little studied, probably due to difficulty of synthesis. More recently a few groups have begun to revisit the $CaCrO_3$ and $SrCrO_3$ compounds.[6–9] Whether these systems are metallic, strongly correlated, and spin ordered is still controversial.[6–10]

Roth and DeVries reported an ordered moment of 1.9 μ_B and Curie-Weiss moment of 2.83 μ_B in the isovalent compound $PbCrO_3$, consistent with $S = 1$ Cr^{4+} (d^2).[1] Chamberland and Moeller synthesized a single crystal, which was semiconducting with 0.27 eV activation energy.[2] There was an anomaly at T_1=240 K, and an upturn at T_2=160 K, in susceptibility. The latter was thought to imply a G-type antiferromagnetic (AFM) ordering corresponding to antiparallel spin ordering between all nearest neighbor Cr^{4+} ions. Additionally, at T_3=100 K, the logarithmic resistivity shows a kink, implying another transition. The samples of both groups had a cubic structure with lattice constant $a \approx$ 4.00 Å. Local spin density approximation (LSDA) calculations obtained a magnetic moment of 1.4 μ_B, three-quarters of the experimental value, but no band-gap.[11] This difference points to interaction effects beyond those described by LSDA. Chamberland also synthesized a cubic $SrCrO_3$ with a=3.818 Å, and concluded it to be a paramagnetic (PM) metal.[3]

Goodenough *et al.* synthesized polycrystalline $CaCrO_3$, which is orthorhombic (a=5.287 Å, b=5.316 Å, and c=7.486 Å) and non-conducting (although probably due to polycrystallinity).[4] Weiher, Chamberland, and Gillson obtained a metallic single crystal sample.[5] The susceptibility measurements showed two anomalies, a kink at 325 K and an upturn at 90 K. At the latter, which is recently identified as the Neel temperature T_N,[6, 9] a kink in the resistivity data and decrease in volume by 2 % from the powder diffraction studies were observed. The Curie-Weiss moment is high spin 3.7 μ_B, recently confirmed by Zhou *et al.*[6] The reason of large difference from spin-only value of 2.8 μ_B for S=1 system is unresolved, however it was found that the susceptibility in $SrCrO_3$ did not follow a Curie-Weiss behavior so no local moment value could be identified.

In more recent studies, Zhou *et al.* observed a smooth decrease in thermal conductivity of $CaCrO_3$ and $SrCrO_3$ compounds as temperature is lowered, in their interpretation characteristic of neither an insulator nor a metal.[6] They interpreted this unusual behavior as due to some unusual Cr–O bonding instability, supported by an increase in compressibility observed around 4 GPa. In contrast to Chamberland's initial suggestion,[3] Zhou *et al.* concluded that $SrCrO_3$ is PM and insulating. Komarek *et al.* reported antiferromagnetism with ordering wavevector $Q_M = (\frac{1}{2}, \frac{1}{2}, 0)$ (in units of $\frac{2\pi}{a}$) and a saturation magnetic moment of 1.2 μ_B, using SQUID susceptibility and neutron diffraction.[9] At

T_N, in contrast to the preliminary observations,[5] no change in volume was apparent. They suggested $CaCrO_3$ is itinerant, but close to being localized, implying importance of correlation effects.[9, 10] Additionally, no evidence of orbital ordering within the t_{2g} shell was observed.[9]

Attfield and coworkers have concentrated on $SrCrO_3$, using neutron diffraction and synchrotron powder x-ray diffraction studies.[7, 8] Below $T_N \approx$40 K, most of their sample underwent a structure transition from a PM cubic phase to a AFM tetragonal phase, but the two phases coexist even at low T. In the tetragonal phase with only slightly inequivalent lattice parameters, at T_N there are no visible changes in volume or in averaged Cr-O distance, and additionally no kink in resistivity. The temperature dependent neutron diffraction data imply orbital reoccupation $(d_{xy}d_{xz}d_{yz})^2 \rightarrow d^1_{xy}(d_{xz}d_{yz})^1$ in the tetragonal phase at or near T_N. Both phases are metallic, though showing high resistivity due to grain boundary scattering.

In this paper, we will focus on $SrCrO_3$, which has been little studied theoretically to date. In Sec. III, in particular, we will address electronic structures of both PM cubic phase and AFM distorted phase, and show that the inclusion of correlation effects leads to an orbital-ordering driven distortion while remaining metallic. In Sec. IV, we discuss the oxygen breathing vibration that shows quite strong magneto-phonon coupling.

II. STRUCTURE AND CALCULATION

Attfield and coworkers suggested a small structure distortion involving relative displacement of Sr and O ions, leading to $\sqrt{2}a \times \sqrt{2}a \times 2a$ quadrupled supercell (space group: $Imma$, No. 74).[7] The corresponding AFM order we consider, which is $(\frac{1}{2}, \frac{1}{2}, \frac{1}{2})$ in terms of the original perovskite cell, will be denoted AFM II. Through more precise measurements, instead of AFM II they more recently concluded a tetragonally distorted structure with $c/a \approx$0.992 but negligible change in volume (less than 1%), which shows antiferromagnetic ordering at wavevector Q_M=($\frac{1}{2}$, $\frac{1}{2}$,0) (space group: $P4/mmm$, No. 123).[8] This structure will be called AFM I. Although this tetragonal phase is dominant below T_N, a nonmagnetic cubic phase also coexists, consistent with results of our calculations (see below).

We investigated both distorted structures as well as the cubic phase, using LSDA and the LDA+Hubbard U (LDA+U) method.[12, 13] For AFM II, only the planar O position is displaced along the $\langle 001 \rangle$ direction, since negligible displacements in Sr and apical O were initially suggested.[7] We used the recent experimental lattice constant a=3.811 Å for the cubic structure and AFM II, and a=3.822 and c=3.792 Å for AFM I.[8] Our optimized lattice constants in the cubic phase within LSDA are 3.748 Å for PM and 3.76 Å for AFM, reflecting the usual small increase in volume associated with magnetism and the overbinding that is common in LSDA.

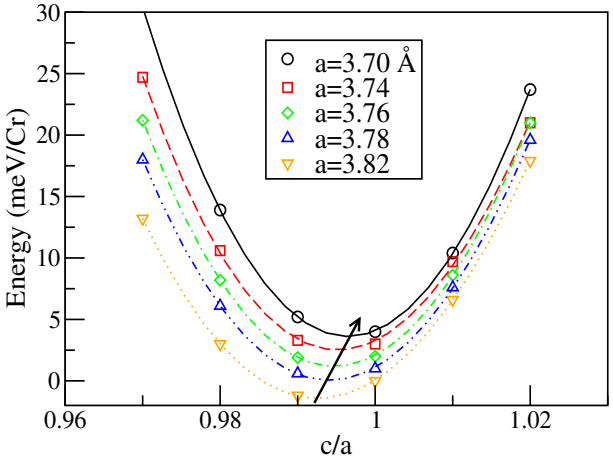

FIG. 1: (Color online) Changes in energy $SrCrO_3$ with respect to lattice parameter ratio (c/a) in AFM I phase, when a volume is fixed for each a parameter. This a parameter is varied in the range of 3.70–3.82 Å , which is approximately the range between our optimized value and the experimentally observed value. Each energy minimum is roughly connected by the arrow, to point out the stronger structural distortion for larger volume.

We have used the full-potential local orbital code FPLO for our study. In FPLO-5,[14] basis orbitals were chosen such as Cr $(3s3p)4s4p3d$, Sr $(4s4p)5s5p4d$, and O $2s2p3d$. (The orbitals in parentheses indicate semicore orbitals.) The Brillouin zone was sampled with a regular mesh containing 726 irreducible k points, since a fine mesh is required for sampling the Fermi surface.

III. ELECTRONIC STRUCTURE

A. Structure Relaxation

Our LSDA calculations show this tetragonally distorted structure (AFM I) is energetically favored over the cubic structure. As expected from the small change in structure, however, the difference in energy is small, no more than 1 meV per Cr. The fact that these two structures are nearly degenerate is consistent with experimental observations. The AFM II phase, on the other hand, has a slightly

higher energy than the cubic phase. In this section, we will focus on only the competing cubic and AFM I phases.

To investigate sensitivity of this structure distortion to volume, we calculated the energy vs. c/a relation in the range of a=3.70–3.82 Å. The volume is kept fixed while the c/a ratio of lattice parameters is varied, since the experiment shows negligible change in volume between two phases.[8] The result is given in Fig. 1. In very close agreement with experimental observations, a minimum occurs at c/a=0.99 for a=3.82 Å, which is the experimentally observed lattice parameter. However, with decreasing volume this distortion is gradually relieved, and finally the cubic structure is favored energetically somewhat below a ≈3.70 Å, 0.06 Å smaller value than our optimized parameter.

B. Energetics

As discussed in the Introduction, the recent observations indicate the coexistence of PM cubic phase and AFM tetragonally distorted phase.[8] Within LSDA, AFM order is more favored energetically than PM in both magnetic structures. The AFM I state is favored energetically over FM by 150 meV/Cr (the moment is 1.55μ_B), whereas the ferromagnetism is only 11 meV/Cr favored over PM even though the moment is 1.16μ_B/Cr. With Stoner I = 0.6 eV (see below), the energy gain due to a simple Stoner instability $IM^2/4$ would lead to much larger value of ∼0.6 eV/Cr for this S = 1 system (the moments are roughly consistent with S=1, in the presence of strong $p-d$ hybridization). The difference in moments reflects considerable hybridization as well, so a fixed-local-moment (*i.e.* Heisenberg picture) is limited in usefulness. The behavior of ferromagnetic order will be investigated more explicitly by fixed spin moment calculations.[15] The energy differences are nearly independent of such a small distortion in structure.

C. PM Cubic Phase within LDA

In this subsection we address the electronic structure of the PM cubic phase (observed above 40 K) using LDA. The band structure around the Fermi level E_F (the Cr d regime) is shown in Fig. 2, and the corresponding densities of states (DOSs) are displayed in Fig. 3. The one-third filled Cr t_{2g} manifold with width of 2 eV lies between –1.5 eV and 0.5 eV (we take E_F as the zero of energy). The unfilled Cr e_g manifold touches the t_{2g} manifold at the X point at 0.5 eV and extends to 4.5 eV, leading to the t_{2g}-

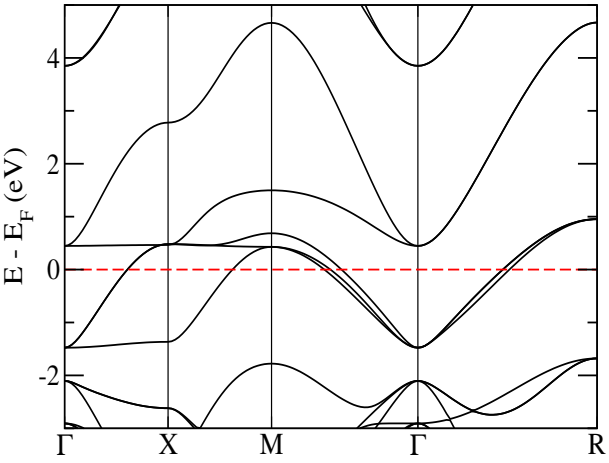

FIG. 2: (Color online) Enlarged band structure of PM $SrCrO_3$ in the regime of Cr d band. A flat band along the $\Gamma - X - M$ line lies at 0.5 eV. The O $2p$ states lie on the regime of –7.5 - –1.8 eV (not shown here). These symmetry points follow a simple cubic notation (see Fig. 4). The R point is a zone boundary along $\langle 111 \rangle$ direction. The horizontal dashed line indicates the Fermi energy E_F.

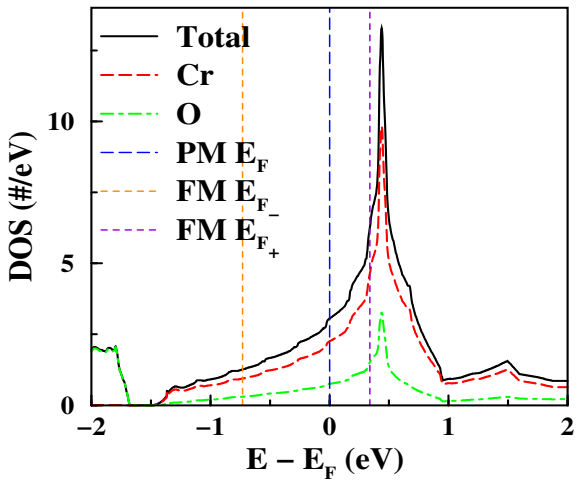

FIG. 3: (Color online) Total and atom-projected densities of states in PM $SrCrO_3$. A sharp peak lies at 0.5 eV. The DOS at E_F N(0) is 1.53 states per eV per spin. A quarter of N(0) is contributed by O ions. Allowing FM ordering, the exchange splitting of t_{2g} states is about 1.1 eV, resulting in total spin moment 1.26 μ_B.

e_g (midpoint) splitting of roughly 2.5 eV. Flat bands along the $\Gamma - X - M$ lines result in a sharp peak in the DOS at 0.5 eV, which otherwise does not have any distinguishing structures near E_F.

The Fermi surfaces shown in Fig. 4 display nesting features, indicative of large susceptibilities at related wavevectors and suggesting the possibility of either magnetic or charge instabilities. The intersecting

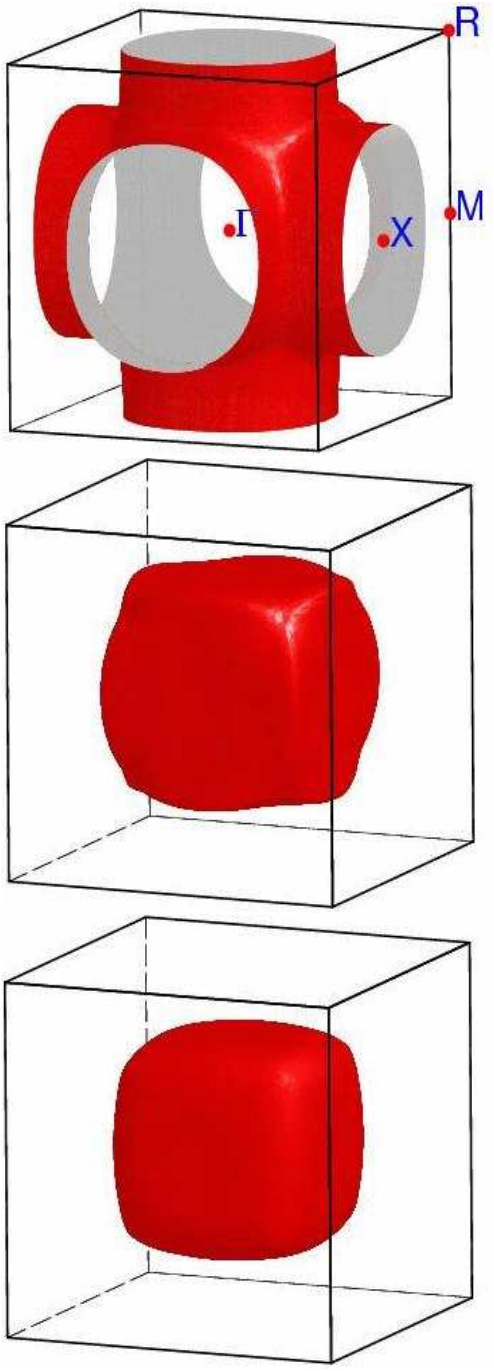

FIG. 4: (Color online) Fermi surfaces, which contain electrons of PM $SrCrO_3$. These surfaces show strong nesting features. Both the second and the third surfaces are cubic-like with rounded edge, but each face of the second surface is circular. The Fermi velocity of 2×10^7 cm/sec, which is a typical value in a metal, is nearly uniform through the surfaces.

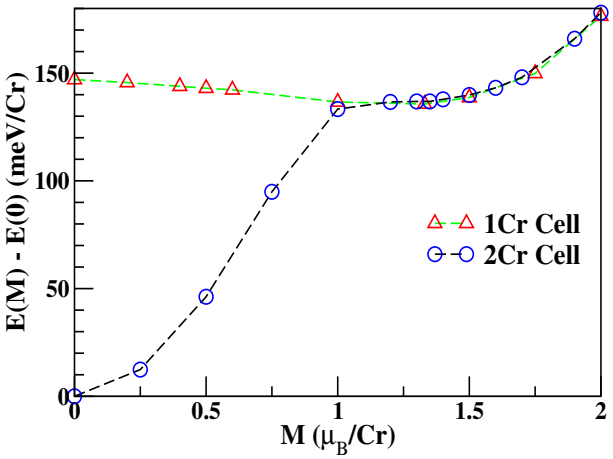

FIG. 5: (Color online) Fixed spin moment calculations using one Cr and two Cr cells. The latter cell allows both PM and AFM states at moment M=0. For the doubled cell, the plot shows richer behavior (see text). Above $1\mu_B$ the states are the same FM state.

pipe-like surface has six circular faces with a radius of $0.32(\frac{\pi}{a})$, so contains ∼0.6 electrons per spin. Two cube-like surfaces with sides of length $\sim0.61(\frac{2\pi}{a})$ are very similar in size, and touch along the $\Gamma - X$ line.

D. Fixed Spin Moment (FSM) Studies

Initially we used a single Cr cell for our calculations, supplementing this with doubled cells (see below). Consistent with our LSDA calculations, E(M) has a minimum at M ∼1.3 μ_B and a related small gain of 11 meV in energy, as can be seen in curve in Fig. 5. The very flat E(M) behavior for M up to $1.5\mu_B$ indicates that magnetism in $SrCrO_3$ is very peculiar. The gain in exchange energy $IM^2/4$ is almost exactly compensated by a cost in other energy contributions across this range. The energy vs. moment curve is fit at small M to the expression $\varepsilon - \varepsilon_0 = \alpha M^2 + \beta M^4$ to evaluate the Stoner (exchange) constant I from these FSM calculations.[15] The resulting value of $\alpha = -17$ meV/μ_B^2 provides the enhanced (observed) susceptibility given by

$$\chi = \frac{\chi_0}{1 - N(0)I} \equiv \mathcal{S}\chi_0, \qquad (1)$$

where the bare susceptibility is $\chi_0 = 2\mu_B^2 N(0)$. The Stoner enhancement factor $\mathcal{S} = [2\alpha\chi_0]^{-1}$ is about -8. Thus the Stoner $I = 0.6$ eV, and $IN(0) = 1.1$ with $N(0) = 1.87$ states per eV per spin from our FM calculations, predicting the system is beyond the Stoner magnetic instability in the cubic phase (within LSDA).

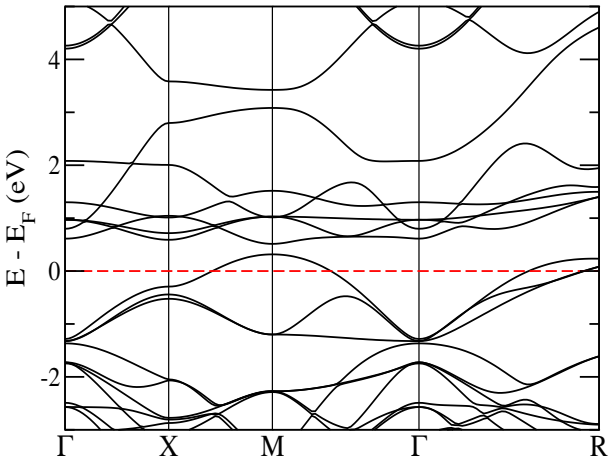

FIG. 6: (Color online) Enlarged band structure of AFM I in the tetragonally distorted structure. That of the cubic phase with the same volume is very similar, so it not shown here. The antiferromagnetism introduces a gap at the X point in the range of –0.5-0.5 eV. For better comparison with PM bandstructure given in Fig. 2, the AFM I Brillouin zone was rotated by 45°.

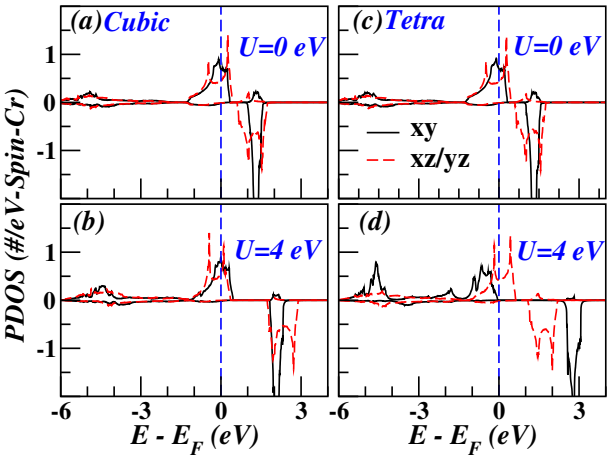

FIG. 7: (Color online) U-dependent orbital-projected densities of states of Cr t_{2g} states for (a)-(b) the cubic and (c)-(d) the tetragonal phase, at U=0 and 4 eV in AFM I. At U=4 eV, an orbit-ordering transition in d_{xy} orbital occurs in the tetragonal phase.

To generalize the study, we used the two-Cr supercell and started from AFM I magnetic order (AFM II magnetic order showed similar change) which also has M=0. A small systematic energy difference between single and doubled cells has been accommodated by aligning the M=0 energies. This energy vs. M curve is comprised of three separate regimes: AFM at $M = 0$ where the energy is ∼150 meV/Cr lower than for PM; ferrimagnetic for $0 < M \leq 1$ where the two Cr moments differ; FM for $M > 1$ where both describe the same simple FM phase. While one might expect strong magneto-elastic coupling in this system, we find that our FSM results are insensitive to c/a ratio in the range given in Fig. 1.

E. LSDA Electronic Structure of the AFM Tetragonally Distorted Phase

Although Attfield and coworkers observed coexistence of the nonmagnetic cubic phase and the antiferromagnetic tetragonal phase, our LSDA calculations show energetically favored AFM in both phases, as already addressed. The AFM I band structure is shown in Fig. 6. The Cr local moment is 1.55 μ_B, with negligible dependence on this small tetragonal distortion. The largest effect of the structure distortion on the band structure occurs in the maxima at the M and R points, downshifting in energy at most 25 meV. The topmost band crossing E_F has the d_{xy} character.

F. Inclusion of Correlation Effects

LSDA predicts the AFM I phase to be considerably lower in energy than the PM phase, in disagreement with experimental data that suggests the two phases are nearly degenerate. We address this discrepancy by including correlation within the LSDA+U approach. On-site Coulomb repulsion U was applied on the Cr ions with AFM order. U was varied in the range of 0–8 eV, but the Hund's exchange integral J=1 eV is fixed since the results in the physical range of U are expected to be insensitive to J.

At U=0=J (i.e., LSDA level), two electrons are evenly distributed in the three bands of the majority t_{2g} manifold. In the AFM I (tetragonal) phase, increasing U changes occupancies, with d_{xz} and d_{yz} weight transferring into d_{xy}. At U_c=4 eV, the majority d_{xy} band is fully occupied, while the majority d_{xz} and d_{yz} bands share equally the other electron, as shown in the orbital-projected DOS given in Fig. 7. This $d^1_{xy}(d_{xz}d_{yz})^1$ state is consistent with Attfield and coworkers' conclusion from their neutron diffraction measurements.[8] This partial orbitally ordered arrangement remains for larger values of U. A potentially Mott-insulating $d^1_{xz}, d^1_{yz}, d^0_{xy}$ state is available but did not arise in the calculations.

An orbital ordering transition in a multi-

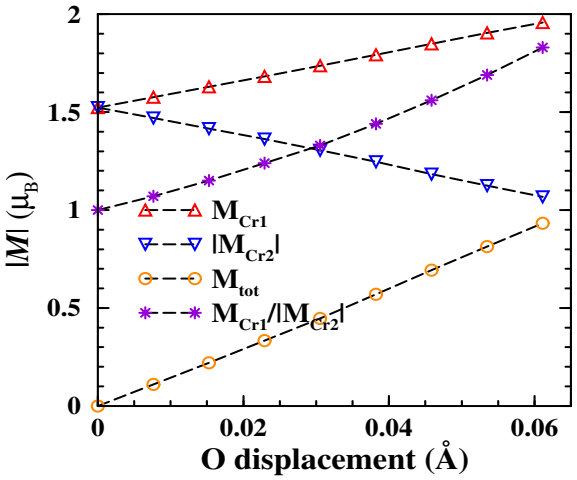

FIG. 8: (Color online) Change in moments due to the O breathing vibration when AFM allows. The Cr1, Cr2, and total moments are changed 7.1, −7.5, and 15.3 μ_B/Å in magnitude. Note that no displacement leads to AFM.

band system can result in significantly different bandwidths.[16] However, in this case, the difference in the occupied bandwidths is small, about 100 meV. The important change is that the center of the d_{xy} band lies roughly 1 eV lower than those of the partially occupied d_{xz}, d_{yz} bands. It is this difference in the band center (*i.e.* the on-site energy) that drives this transition, as happened in Na_xCoO_2 [17] or V_2O_3.[18] Keeping the structure (and symmetry) cubic inhibits such an orbital-ordering transition.

IV. O TILTING AND BREATHING PHONON MODES

To investigate another possibility of structure distortion in this perovskite, we used AFM II order, which allows O tilting and breathing phonon modes in frozen phonon calculations. However, our calculations show these distortions are unfavored energetically, resulting in stable phonon modes. First, for the O tilting vibration the phonon energy is 38 meV, typical for metallic oxides. For the breathing mode the energy is 89 meV, corresponding to an *rms* displacement of the oxygen ions by 0.05 Å. (Allowing magnetic ordering, both frequencies reduce by $\sim$ 5%.) This frequency corresponds to an *rms* displacement of 0.05 Å.

Our calculations show strong magneto-phonon coupling for the breathing mode. When AFM ordering is included, the Cr local moment of M_{Cr}=1.5 μ_B is modulated by about $\pm$7.3 μ_B/Å, as shown in Fig. 8. These changes are quite large, even larger than the change in Fe moment, 6.8 μ_B/Å, in LaFeAsO when As ions are displaced, which is widely discussed as unusually strong magneto-phonon coupling.[19] At the *rms* displacement, the difference between Cr moments becomes 0.73 μ_B, illustrating just how large the modulation of the moment by the breathing mode is. The Cr charge "disproportionation" due to O breathing also shows a value of $\pm 0.13e$ (*i.e.* a $0.26e$ charge difference) at the *rms* displacement, corresponding to a shift in charge of $\pm 2.6e$/Å.

V. SUMMARY

We have presented and analyzed the electronic structure, magnetic ordering, and the impact of strong correlation effects in the perovskite material $SrCrO_3$, which is reported in a paramagnetic cubic phase coexisting with an antiferromagnetic phase concurrent with a small distortion in structure below 40 K. Consistent with these observations, LSDA predicts the slightly distorted tetragonal structure, but overestimates the polarization energy. With LSDA the cubic phase is magnetically unstable, with a Stoner product $IN(0)$ $\approx$1.1. The Fermi surface shows nesting features, but they do not correlate with known data.

Including correlated effects within the LDA+U approach, the distorted phase undergoes an orbital ordering transition at a critical interaction strength U_c=4 eV, leading to $t_{2g}^2 \rightarrow d_{xy}^1(d_{xz}d_{yz})^1$ orbital ordering and structural transition to tetragonal structure. The structural symmetry lowering is crucial; the cubic phase remains a simple metal even for higher U. We have also demonstrated that the O breathing modes show strong magneto-phonon coupling.

The magnetic behavior in $SrCrO_3$ remains unclear. The experimental data show weak magnetic behavior,[8] and the susceptibility does not follow Curie-Weiss behavior.[6] In contrast to these observations, our various calculations always result in a full moment corresponding to S=1 configuration (reduced by hybridization) as expected for a d^2 ion. Without any peak in the DOS, the temperature variation cannot be modeled with temperature broadening as can be done, for example, in $TiBe_2$.[20]

VI. ACKNOWLEDGMENTS

We acknowledge important communications with J. P. Attfield concerning his experimental observations, J.-S. Zhou for clarifying structure of $CaCrO_3$, and A. Kyker for illuminating discussion of tem-

perature dependent susceptibility. This work was supported by DOE under Grant No. DE-FG03-01ER45876, and interaction within DOE's Computational Materials Science Network is acknowledged. K.W.L. was partially supported by a Korea University Grant No. K0718021.

[1] W. L. Roth and R. C. DeVries, J. Appl. Phys. **38**, 951 (1967); R. C. DeVries and W. L. Roth, J. Am. Ceram. Soc. **51**, 72 (1968).
[2] B. L. Chamberland and C. W. Moeller, J. Solid State Chem. **5**, 39 (1972).
[3] B. L. Chamberland, Solid State Commun. **5**, 663 (1967).
[4] J. B. Goodenough, J. M. Longo, and J. A. Kafalas, Mat. Res. Bull. **3**, 471 (1968).
[5] J. F. Weiher, B. L. Chamberland, and J. L. Gillson, J. Solid State Chem. **3** 529 (1971).
[6] J.-S. Zhou, C.-Q. Jin, Y.-W. Long, L.-X. Yang, and J. B. Goodenough, Phys. Rev. Lett. **96**, 046408 (2006).
[7] A. J. Williams, A. Gillies, J. P. Attfield, G. Heymann, H. Huppertz, M. J. Martínez-Lope, and J. A. Alonso, Phys. Rev. B **73**, 104409 (2006).
[8] L. Ortega-San-Martin, A. J. Williams, J. Rodgers, J. P. Attfield, G. Heymann, and H. Huppertz, Phys. Rev. Lett. **99**, 255701 (2007).
[9] A. C. Komarek, S. V. Streltsov, M. Isobe, T. Moller, M. Hoelzel, A. Senyshyn, D. Trots, M. T. Fernández-Díaz, T. Hansen, H. Gotou, T. Yagi, Y. Ueda, V. I. Anisimov, M. Gruninger, D. I. Khomskii, and M. Braden, Phys. Rev. Lett. **101**, 167204 (2008).
[10] S. V. Streltsov, M. A. Korotin, V. I. Anisimov, and D. I. Khomskii, Phys. Rev. B **78**, 054425 (2008).
[11] S. Mathi Jaya, R. Jagadish, R. S. Rao, and R. Asokamani, Mod. Phys. Lett. B **6**, 103 (1992).
[12] V. I. Anisimov, I. V. Solovyev, M. A. Korotin, M. T. Czyzyk, and G. A. Sawatzky, Phys. Rev. B **48**, 16929 (1993).
[13] M. T. Czyzyk and G. A. Sawatzky, Phys. Rev. B **49**, 14211 (1994).
[14] K. Koepernik and H. Eschrig, Phys. Rev. B **59**, 1743 (1999).
[15] K. Schwarz and P. Mohn, J. Phys. F **14**, L129 (1984).
[16] R. Arita and K. Held, Phys. Rev. B 72, 201102(R) (2005).
[17] K.-W. Lee, J. Kunes, and W. E. Pickett, Phys. Rev. B **70**, 045104 (2004); K.-W. Lee, J. Kunes, P. Novak, and W. E. Pickett, Phys. Rev. Lett. **94**, 026403 (2005).
[18] M. S. Laad, L. Craco, and E. Müller-Hartmann, Phys. Rev. B **73**, 045109 (2006).
[19] Z. P. Yin, S. Lebègue, M. J. Han, B. P. Neal, S. Y. Savrasov, and W. E. Pickett, Phys. Rev. Lett. **101**, 047001 (2008).
[20] T. Jeong, A. Kyker, and W. E. Pickett, Phys. Rev. B **73**, 115106 (2006).